Applied Physics Letters

RESEARCH ARTICLE | DECEMBER 08 2025

Direct measurement of the electron wind force in cobalt nanowires

Brian Zutter ; Matthew Mecklenburg ; Yueyun Chen ; Ho Leung Chan ; Jared J. Lodico ;
B. C. Regan

Appl. Phys. Lett. 127, 231901 (2025)
https://doi.org/10.1063/5.0304171

AIP Publishing

Direct measurement of the electron wind force in cobalt nanowires

Cite as: Appl. Phys. Lett. **127**, 231901 (2025); doi: 10.1063/5.0304171
Submitted: 26 September 2025 · Accepted: 20 November 2025 ·
Published Online: 8 December 2025

View Online Export Citation CrossMark

Brian Zutter,[1] Matthew Mecklenburg,[2,3,a)] Yueyun Chen,[1] Ho Leung Chan,[1] Jared J. Lodico,[1] and B. C. Regan[1,a)]

AFFILIATIONS

[1]Department of Physics & Astronomy and California NanoSystems Institute, University of California, Los Angeles, California 90095, USA
[2]Core Center of Excellence in Nano Imaging, University of Southern California, Los Angeles, California 90089, USA
[3]California NanoSystems Institute, University of California, Los Angeles, California 90095, USA

[a)]Authors to whom correspondence should be addressed: mmecklenburg@cnsi.ucla.edu and regan@physics.ucla.edu

ABSTRACT

Copper back-end-of-line interconnects have been the industry standard for decades, but copper's susceptibility to electromigration failure has motivated a search for alternatives. While cobalt's resistivity is higher than copper's in bulk form, it scales more slowly with decreasing interconnect size, making cobalt a promising alternative for highly scaled interconnects. To better understand the electromigration behavior of cobalt, we map both temperature- and the current-induced strain in cobalt nanowires using a scanning transmission electron microscope equipped with an electron energy loss spectrometer. We consistently see cobalt move away from the anode, and we find cobalt's effective ionic charge $Z^* = +2 \pm 1$ near 300 °C. This result will inform the design of highly scaled cobalt interconnects.

Copper is the current industry standard back-end-of-line interconnect material (BEOL).[1] Compared to aluminum, the previous industry standard, copper has higher electrical conductivity, thermal conductivity, and superior resistance to electromigration (EM) failure. However, as the critical dimension of transistors, and thus first-level BEOL interconnects, continues to decrease, the effective conductivity of copper decreases due to surface and grain boundary scattering.[2,3] Furthermore, copper interconnects require barrier and adhesion layers, which decrease its effective conductivity at small critical dimensions.[1,4]

Cobalt is being investigated as a next-generation interconnect material. Cobalt's carrier mean-free-path is shorter than copper's, and its bulk electrical conductivity is lower. However, because its mean-free-path is short, cobalt's effective electrical conductivity scales more slowly with the interconnect cross-sectional area.[5,6] Cobalt's activation energy of 1.89 eV is also higher than copper's 1.11 eV, which means cobalt is more resistant to electromigration than copper at elevated temperatures.[2] Moreover, cobalt may require fewer diffusion and adhesion liner layers than copper, and therefore would be subject to a smaller liner volume penalty.[1,7] For these reasons, cobalt was incorporated into the first layer of metallization, "M0," at Intel's 10 nm process node.[8]

According to the standard model[9] of electromigration, the ion current density J is given by

$$J = \frac{Z^* e \rho j D_0}{kT} e^{-Q/kT}, \tag{1}$$

where ρ is the material's resistivity, j is the electrical current density, kT is the thermal energy, Q is the activation energy of the ion, and D_0 is its self-diffusion coefficient. The effective ion charge Z^* is a critical parameter for determining how resistant a material is to EM. Cobalt's Z^* has been measured as $Z^* = 1.6 \pm 0.3$ in the temperature range 1260–1360 °C (Ref. 10) and $-13 < Z^* < -0.05$ in the range 360–615 °C (Ref. 11), which suggests that cobalt's Z^* switches from negative to positive between 615 and 1260 °C (Ref. 11). More recently, cobalt's Z^* has been observed to be positive at 790 and 925 °C, and negative at 525 and 625 °C (Ref. 12). Cobalt's Z^* has not been measured below 360 °C, which is the temperature range most relevant to microprocessors. Given cobalt's potential to replace copper in highly scaled interconnects, new data in this temperature range are particularly timely.[13]

Cobalt's electrical conductivity $\sigma = 1/\rho$ and thermal conductivity κ are $\sim 4\times$ lower than copper's, and the temperature change produced by Joule heating scales as $\Delta T \propto j^2/\sigma\kappa$. Thus, at the same electrical current density j, the temperature shifts in cobalt are both larger and more nonuniform than in copper. Because the EM mass transport J depends exponentially upon the temperature [Eq. (1)], knowledge of the temperature distribution across an interconnect is crucial for predicting robustness to EM. Unfortunately, electrical transport measurements can only provide spatially averaged thermometry, and the size of nanoscale interconnects is below the diffraction limit for infrared thermometry.[14] In this work, to extract a value for cobalt's effective ionic charge, Z^*, we map temperature- and EM-induced strain in cobalt nanowires using electron energy loss spectroscopy (EELS) in scanning transmission electron microscope (STEM).

Plasmon energy expansion thermometry (PEET) is an EELS-based STEM technique that has been used to measure temperature in aluminum,[14–16] silicon,[17] molybdenum disulfide,[18] silicon nitride,[19] and indium.[20] A material's bulk plasmon energy is given by

$$E_p = \hbar\omega_p = \hbar\sqrt{\frac{e^2 n}{\epsilon_0 m}}, \tag{2}$$

where $\hbar$ is the reduced Planck constant, ϵ_0 is the permittivity of free space, e is the electron charge, and m is the electron mass, all of which are constant. The valence electron density n varies with temperature because of thermal expansion. If the material can expand freely and the temperature change $\Delta T = T - T_0$ is small [so that the linear thermal expansion coefficient $\alpha(T) \simeq \alpha_1$ is approximately constant], then[20]

$$\Delta T \simeq -\frac{2}{3}\frac{\Delta E_p}{\alpha_1 E_p}. \tag{3}$$

Thus, measurements of changes in the plasmon energy ΔE_p can be related to changes of the temperature via the thermal expansion coefficient. In cobalt, the thermal expansion coefficient[21,22] $\alpha_1 = 13 \times 10^{-6}$/K and the plasmon energy is $E_p = 27$ eV, so PEET's temperature sensitivity $\Delta T/\Delta E_p \simeq -1.9$ K/meV.

An electrical current density j in a wire induces a strain (and concomitant volume change) proportional to j^2 via Joule heating. It also induces a strain proportional to j via the electron wind force. The wind force strain is derived from the current-induced pressure,[15]

$$P(x) = \frac{Z^* e\rho}{\Omega} x j(x), \tag{4}$$

where Ω is the atomic volume.

The Joule heating and wind force strain signals can be separated by exploiting their different symmetries with respect to the electric current's polarity. We construct plasmon energy maps based on the relative difference of a bias-on map and a bias-off map: $R = (E_P - E_{P0})/E_{P0} \simeq \Delta n/2n_0$. We then construct linear combinations of $R(+I) + R(-I) = \Delta n_{\text{even}}/n_0$ and $R(+I) - R(-I) = \Delta n_{\text{odd}}/n_0$. Temperature maps are extracted from $\Delta n_{\text{even}}/n_0 = -3\alpha_1\Delta T$ and wind force strain maps are extracted from $\Delta n_{\text{odd}}/n_0 = P/3B$, where B is cobalt's bulk modulus.[15]

We pattern polycrystalline cobalt nanowires (30 nm thick, 100 nm wide) on electron-transparent (20 nm thick) silicon nitride membranes [Fig. 1(a)] using standard e-beam lithography and metal evaporation techniques. The 4-wire geometry allows the cobalt resistivity to be determined at the center of the nanowire, where the temperature increase due to Joule heating is uniform.

We acquire EELS spectrum images of the indicated region-of-interest [dashed-red box, Fig. 1(a)] in a cobalt nanowire. EELS data are acquired at the National Center for Electron Mircoscopy using the TEAM 1.0 STEM, which is equipped with a Gatan Continuum spectrometer. The data are acquired at 80 keV beam energy. The spherical aberration corrector and the monochromator are not in use. The EELS energy resolution is 0.8 eV. A representative cobalt spectrum [Fig. 1(c)] shows the zero-loss peak (ZLP), the first plasmon, and the $M_{2,3}$ core-loss excitation.

The cobalt plasmon energy is defined as the distance between the ZLP and the cobalt plasmon peak centers. The peak centers are determined with a nonlinear fitting procedure.[20] Briefly, the spectrum image is preprocessed in Gatan DigitalMicrograph 3 for a rough ZLP

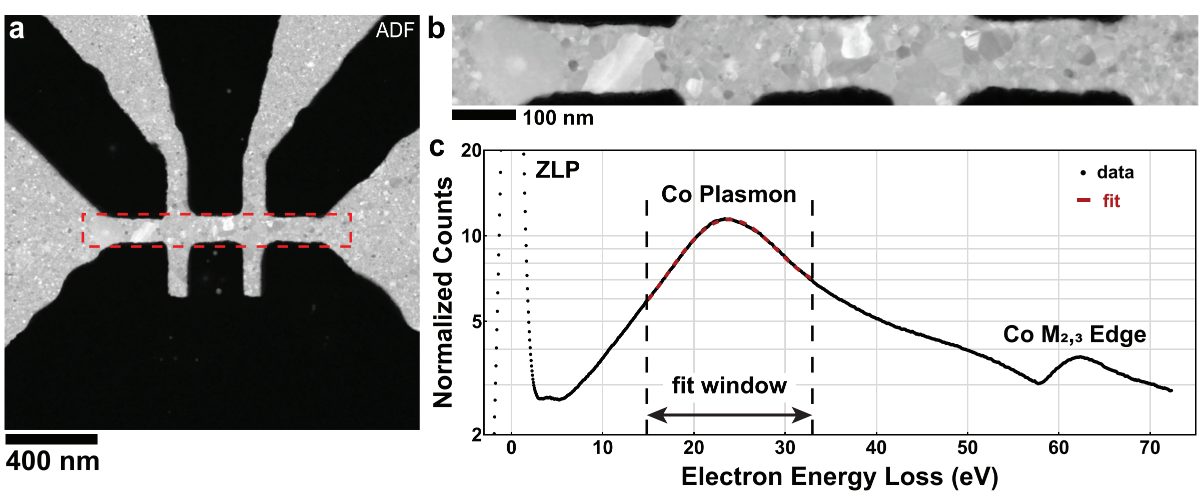

FIG. 1. Device architecture and EELS spectra. Low-magnification (a) and high-magnification (b) STEM ADF images of a cobalt nanowire supported on a silicon nitride membrane. (c) EELS spectrum of cobalt, with Gaussian curve fitting applied to a localized window centered around the plasmon resonance.

alignment. Then, for each real-space pixel in the energy-space-aligned spectrum image, the ZLP region (−0.75–0.75 eV) and the low-loss region (15–33 eV) are separately fit to a function consisting of a Gaussian with a linear background [Fig. 1(c)]. The distance between the two Gaussian peak centers is taken as the energy of the cobalt plasmon at the given real-space pixel. Our ability to precisely determine this plasmon energy is primarily limited by the plasmon peak's native width and the total signal (i.e., beam current), which is why we do not use the monochromator.

Maps of the plasmon energy determined by this fit procedure show grain boundaries in the cobalt wire [Fig. 2(a)]. Imperfect atomic packing at grain boundaries decreases the electron density relative to the grain interior. The fact that we resolve these drops demonstrates that this technique's spatial resolution approaches the atomic scale.[14] It also highlights the need to compare bias-on measurements with bias-off measurements performed in the same region. The grain structure varies from place to place inside the wire, with concomitant variation in the plasmon energy. This variation is not small compared to the temperature- and pressure-induced changes created by an applied bias. Thus, the bias-induced plasmon energy changes can only be identified by subtracting off the zero-bias plasmon energy maps (Fig. 2).

While cobalt's plasmon energy can be used to determine temperature- and wind force-induced pressure in principle, several factors make these determinations challenging in practice. Cobalt's plasmon peak is broad in comparison to, say, aluminum's[14] or indium's,[20] which makes it more difficult to measure the central energy precisely. The cobalt peak range (10–50 eV) also overlaps that of the silicon nitride (the membrane window) and carbon (contamination) plasmons [Fig. S1(b)], making it difficult to measure the change in central energy accurately. Due to the nonuniform distribution of the carbon contamination, a naïve determination of the cobalt plasmon energy shift would be corrupted by the change in the amplitude of the cobalt plasmon relative to the carbon plasmon. To mitigate this systematic error, multiple linear least squares (MLLS) fitting is used to generate a mask that confines our attention to regions that have cobalt and do not have heavy carbon contamination [Fig. S1(d)].

Under bias, the plasmon energy drops across the entire map because of Joule heating across the field of view. Plasmon energy profiles derived from the $I = \pm 1.4$ mA bias maps (after masking) are approximately 200 meV lower than the $I = 0$ maps [Fig. 2(b)]. Converted into a temperature shift with Eq. (3), this plasmon energy shift implies a $\Delta T = 400$ K at the center of the nanowire [Fig. 3(a)]. The temperature change introduced by Joule heating is consistent between bias polarities, since the power density dissipated within the nanowire is polarity-independent. The temperature drops symmetrically away from the midpoint, falling by 40 K at the limits of the field

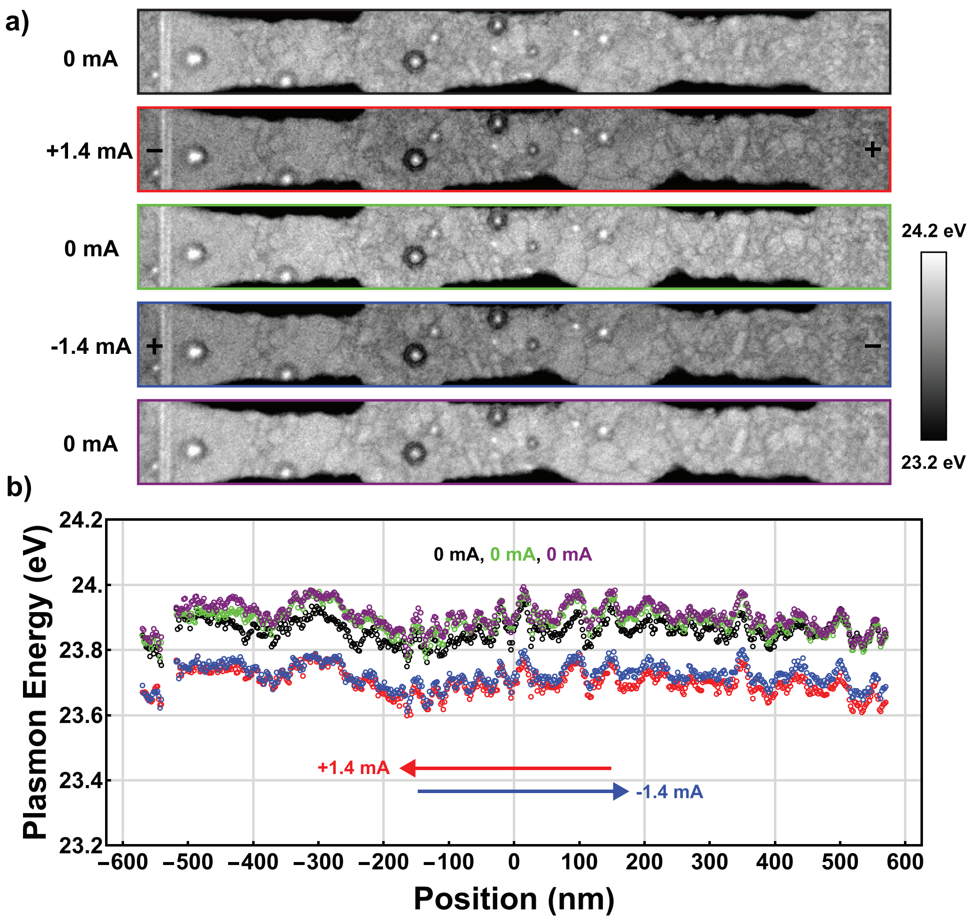

FIG. 2. Cobalt plasmon energy maps. Cobalt plasmon energy maps (a) acquired at ± 1.4 mA current have a plasmon energy $\sim$200 meV lower than the reference zero-bias images due to thermal expansion caused by Joule heating. Line profiles (with colors corresponding to the image borders above) representing averages across the nanowire's width (b) reveal a slight difference in plasmon energy between the $+1.4$ mA and -1.4 mA image, due to wind force-induced strain. Regions with no cobalt (dark) or heavy carbon contamination (bright) are excluded from the averaging (see masking in Figs. 3 and S1).

of view [Fig. 3(a)]. This drop is expected because the greater width of the 4-wire source leads makes them more effective heat sinks than the sense leads.

The temperature of the wire can be independently estimated using 4-wire transport data acquired over the course of the experiment (Fig. S2). These measurements yield $\Delta T \simeq 250$ K for both positive and negative bias, ∼40% lower than the EELS-derived measurement. This discrepancy indicates the presence of systematic errors in the transport temperature determination, the PEET temperature determination, or both.

Our simplifying assumptions could compromise one or both of these temperature determinations. Neglecting the silicon nitride membrane's contributions to the EELS spectrum introduces an error in PEET to the extent that silicon nitride and cobalt have different thermal expansion coefficients and the membrane thickness is nonzero. Neglecting the width of the sense leads introduces an error in the transport thermometry to the extent that the potential they sample is not equal to the potential on their midlines.

Cobalt has an hcp to fcc phase transition that could potentially impact both measurements. The 700 K transition temperature seen in the bulk[23] can occur at lower temperatures in thin-films.[24] This phase transition introduces a 0.3% change in density[22] and a 6% drop in resistivity.[23] We see no sign of such changes and the transition is

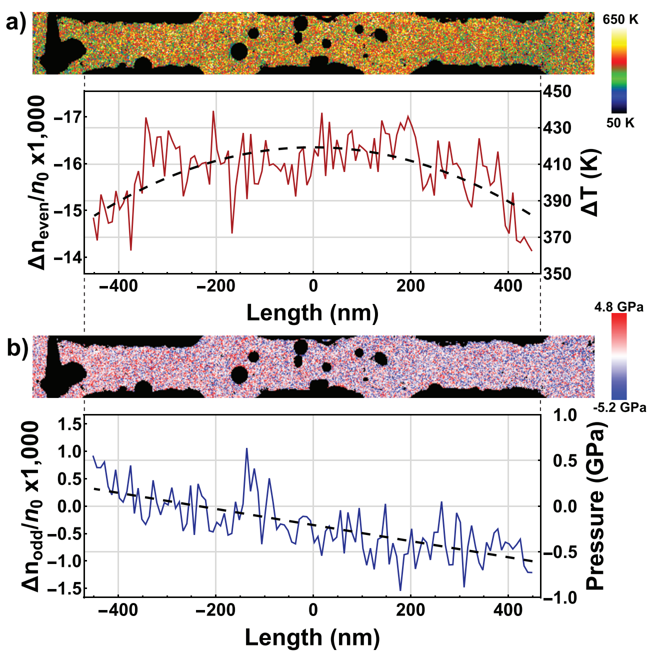

FIG. 3. Temperature and pressure profiles along the length of the nanowire. (a) The even-polarity component, $\Delta n_{even}/n_0$, of the change in electron density with bias (left ordinate) is used to calculate ΔT along the nanowire axis (right ordinate). A parabola is fit (black dashed curve) to the ΔT profile, with a peak of approximately 400 K. (b) The odd-polarity component, $\Delta n_{odd}/n_0$, of the change in electron density with bias (left ordinate) is used to calculate the electron wind force pressure along the nanowire axis (right ordinate). A line is fit (black dashed line) to the pressure profile, with a slope of approximately -0.9 MPa/nm. The dark regions inside the wire in both maps above are not voids, but rather regions that have been masked off because of carbon contamination. (Compare the maps of Fig. 2.)

perhaps beyond the upper end of the likely temperature range, so we assume that the sample does not make it.

To further investigate the thermometry discrepancy, we apply PEET to the bare silicon nitride[19] adjacent to the cobalt (Fig. S3). Here, PEET gives $\Delta T = 260$ K, which is a close match to the transport-derived temperature measurement. In addition, a finite-element steady-state thermal simulation (Fig. S4) gives a maximum temperature of 300 K above room-temperature at 1.4 mA bias.

We thus have four different methods for determining the temperature. These give values for ΔT ranging from 250 K (transport) to 260 K (PEET silicon nitride) to 300 K (simulation) to 420 K (PEET cobalt). Given these discrepant results, we estimate $\Delta T \sim 300$ K.

As the current-polarity-even effect in the plasmon energy gives the temperature, the current-polarity-odd effect gives the wind force-induced strain. Using the odd linear combination of the same EELS maps used to extract temperature, we find the pressure using $P = 3B\Delta n_{odd}$. A linear fit of the strain values [Eq. (4)] gives a measurement of $Z^* = +2$ [Fig. 3(b)]. However, a systematic error in the PEET temperature measurement would imply an error in the strain determination, which would produce a corresponding error in our determination of Z^*. Since we do not fully understand the errors in our determination of ΔT, we are conservatively assigning a 50% error to our determination Z^*, with the result $Z^* = 2 \pm 1$.

Given these uncertainties, we conducted additional experiments tracking thickness changes with EELS in cobalt during biasing (Fig. S5, and Ref. 25). The positive effective ionic charge indicates that the "direct" force dominates the electron wind, or, alternatively, that holes are the dominant source of momentum transfer from the electric current to the cobalt lattice. We consistently see that cobalt is removed preferentially from the anode (the positive electrode) by biasing, which is consistent with a positive value of Z^*.

Extracting a value of Z^* using changes in wire thickness is challenging because the movement of cobalt ions (J) depends proportionally on cobalt's self-diffusion coefficient D_0 [Eq. (1)] and exponentially on the activation energy and temperature, all three of which contain significant uncertainty. In fact, the ability of this EELS-based technique to measure strain, and therefore Z^*, directly, without complications from D_0, etc., distinguishes the present study from previous work and was an important motivating factor.

In summary, we have biased cobalt nanowires inside a STEM with a current density of 5×10^7 A/cm^2 and an electric field of 100 kV/m. Using STEM EELS, we simultaneously mapped the Joule heating and the strain induced by the applied electrical current. We find positive $Z^* = +2 \pm 1$ at a wire temperature ∼300 °C. Compared to prior measurements[10,11,26] of Z^*, these results concern lower temperature (which is more relevant to microprocessor design) and higher current densities (by more than 10×). We see no evidence of $Z^* < 0$, which has been reported previously.[11,12,26] In fact, the cobalt nanowires tested invariably failed near the anode, indicative of a positive Z^*. This direct measurement of Z^* in a nanoscale cobalt wire will help elucidate cobalt's complex EM behavior and guide the design of next-generation BEOL interconnects.

See the supplementary material for discussion and figures concerning the masking of carbon contamination, temperature determination via transport, PEET on SiN, and finite-element simulations, and tracking cobalt electromigration with EELS thickness mapping.

This work was supported by the Semiconductor Research Corporation (SRC), the National Science Foundation (NSF) Award No. DMR-1611036, and the NSF STC Award No. DMR-1548924 (STROBE). Data were collected at the Core Center of Excellence in Nano Imaging (University of Southern California) and the National Center for Electron Microscopy at Lawrence Berkeley National Lab. Work at the Molecular Foundry was supported by the Office of Science, Office of Basic Energy Sciences, of the U.S. Department of Energy under Contract No. DE-AC02-05CH11231. Samples were fabricated in the Integrated Systems Nanofabrication Cleanroom (ISNC) at the California NanoSystems Institute (CNSI). We thank Jim Ciston, Rohan Dhall, and Karen Bustillo at NCEM for their technical assistance and advice. We also thank Lei Jiang and Ilya Karpov at Intel Corp. for valuable discussions.

AUTHOR DECLARATIONS

Conflict of Interest

The authors have no conflicts to disclose.

Author Contributions

Brian Zutter, Matthew Mecklenburg, and Yueyun Chen contributed equally to this work.

Brian Zutter: Conceptualization (equal); Data curation (equal); Formal analysis (equal); Validation (equal); Visualization (equal); Writing – original draft (equal); Writing – review & editing (equal). **Matthew Mecklenburg:** Conceptualization (equal); Data curation (equal); Funding acquisition (equal); Investigation (equal); Methodology (equal); Project administration (equal); Supervision (equal); Validation (equal); Writing – review & editing (equal). **Yueyun Chen:** Data curation (equal); Formal analysis (equal); Validation (equal); Visualization (equal); Writing – review & editing (equal). **Ho Leung Chan:** Data curation (equal); Writing – review & editing (equal). **Jared J. Lodico:** Data curation (equal); Writing – review & editing (equal). **B. C. Regan:** Conceptualization (equal); Funding acquisition (equal); Investigation (equal); Project administration (equal); Supervision (equal); Writing – review & editing (equal).

DATA AVAILABILITY

The data that support the findings of this study are available from the corresponding author upon reasonable request.

REFERENCES

[1] C.-L. Lo, B. A. Helfrecht, Y. He, D. M. Guzman, N. Onofrio, S. Zhang, D. Weinstein, A. Strachan, and Z. Chen, "Opportunities and challenges of 2D materials in back-end-of-line interconnect scaling," J. Appl. Phys. **128**, 080903 (2020).

[2] F. Griggio, J. Palmer, F. Pan, N. Toledo, A. Schmitz, I. Tsameret, R. Kasim, G. Leatherman, J. Hicks, A. Madhavan, J. Shin, J. Steigerwald, A. Yeoh, and C. Auth, "Reliability of dual-damascene local interconnects featuring cobalt on 10 nm logic technology," in *IEEE International Reliability Physics Symposium (IRPS)* (IEEE, 2018).

[3] D. Gall, "The search for the most conductive metal for narrow interconnect lines," J. Appl. Phys. **127**, 050901 (2020).

[4] J. S. Clarke, C. George, C. Jezewski, A. M. Caro, D. Michalak, and J. Torres, "Process technology scaling in an increasingly interconnect dominated world," in Symposium on VLSI Technology (VLSI-Technology): Digest of Technical Papers (2014).

[5] M. H. van der Veen, N. Heyler, O. V. Pedreira, I. Ciofi, S. Decoster, V. V. Gonzalez, N. Jourdan, H. Struyf, K. Croes, C. J. Wilson, and Z. Tőkei, "Damascene benchmark of Ru, Co and Cu in scaled dimensions," in *IEEE International Interconnect Technology Conference (IITC)* (IEEE, 2018), pp. 172–174.

[6] N. Bekiaris, Z. Wu, H. Ren, M. Naik, J. H. Park, M. Lee, T. H. Ha, W. Hou, J. R. Bakke, M. Gage, Y. Wang, and J. Tang, "Cobalt fill for advanced interconnects," in *IEEE International Interconnect Technology Conference (IITC)* (IEEE, 2017).

[7] B. Engler and R. Hull, "Accelerated electromigration study of cobalt thin films by in-situ TEM," Microsc. Microanal. **25**, 1902–1903 (2019).

[8] A. Yeoh, A. Madhavan, N. Kybert, S. Anand, J. Shin, M. Asoro, S. Samarajeewa, J. Steigerwald, C. Ganpule, M. Buehler, A. Tripathi, V. Souw, M. Haran, S. Nigam, V. Chikarmane, P. Yashar, T. Mulé, Y. Wu, K. Lee, M. Aykol, K. Marla, P. Sinha, S. Kirby, H. Hiramatsu, W. Han, M. Mori, M. Sharma, H. Jeedigunta, M. Sprinkle, C. Pelto, M. Tanniru, G. Leatherman, K. Fischer, I. Post, and C. Auth, "Interconnect stack using self-aligned quad and double patterning for 10 nm high volume manufacturing," in *IEEE International Interconnect Technology Conference (IITC)* (IEEE, 2018), pp. 144–147.

[9] I. A. Blech and E. S. Meieran, "Electromigration in thin Al films," J. Appl. Phys. **40**, 485–491 (1969).

[10] P. S. Ho, "Electromigration and Soret effect in cobalt," J. Phys. Chem. Solids **27**, 1331–1338 (1966).

[11] G. J. van Gurp, "Electromigration and Hall effect in cobalt films," J. Phys. Chem. Solids **38**, 627–633 (1977).

[12] B. Engler and R. Hull, "High temperature electromigration behavior of cobalt lines observed by in situ transmission electron microscopy," Appl. Phys. Lett. **123**, 083502 (2023).

[13] Y.-c. Liu, B. Afflerbach, R. Jacobs, S.-k. Lin, and D. Morgan, "Exploring effective charge in electromigration using machine learning," MRS Commun. **9**, 567–575 (2019).

[14] M. Mecklenburg, W. A. Hubbard, E. R. White, R. Dhall, S. B. Cronin, S. Aloni, and B. C. Regan, "Nanoscale temperature mapping in operating microelectronic devices," Science **347**, 629–632 (2015).

[15] M. Mecklenburg, B. T. Zutter, X. Y. Ling, W. A. Hubbard, and B. C. Regan, "Visualizing the electron wind force in the elastic regime," Nano Lett. **21**, 10172–10177 (2021).

[16] B. Zutter, M. Mecklenburg, S. Aloni, and B. C. Regan, "Electromigration of copper in lithographically-defined aluminum nanowires," Microsc. Microanal. **24**, 2190–2191 (2018).

[17] M. Mecklenburg, B. Zutter, and B. C. Regan, "Thermometry of silicon nanoparticles," Phys. Rev. Appl. **9**, 014005 (2018).

[18] L. Shen, M. Mecklenburg, R. Dhall, B. C. Regan, and S. B. Cronin, "Measuring nanoscale thermal gradients in suspended MoS_2 with STEM-EELS," Appl. Phys. Lett. **115**, 153108 (2019).

[19] B. Zutter, M. Mecklenburg, and B. C. Regan, "Temperature dependence of the silicon nitride volume plasmon," Microsc. Microanal. **22**, 1574–1575 (2016).

[20] W. A. Hubbard, M. Mecklenburg, J. J. Lodico, Y. Chen, X. Y. Ling, R. Patil, W. A. Kessel, G. J. K. Flatt, H. L. Chan, B. Vareskic, G. Bal, B. Zutter, and B. C. Regan, "Electron-transparent thermoelectric coolers demonstrated with nanoparticle and condensation thermometry," ACS Nano **14**, 11510–11517 (2020).

[21] Y. Kasamatsu, M. Koyama, K.-i. Masumoto, K.-i. Kojima, T. Hihara, and T. Kamigaichi, "Dilatometric measurement of the thermal expansion of cobalt single crystal," Jpn. J. Appl. Phys., Part 1 **20**, 37 (1981).

[22] R. N. Abdullaev, R. A. Khairulin, Y. M. Kozlovskii, and S. V. Stankus, "Density and thermal expansion of high purity cobalt over the temperature range from 140 K to 2073 K," Metall. Mater. Trans. A **52**, 5449–5456 (2021).

[23] M. J. Laubitz and T. Matsumura, "Transport properties of the ferromagnetic metals. I. Cobalt," Can. J. Phys. **51**, 1247–1256 (1973).

[24] C. Cabral, K. Barmak, J. Gupta, L. A. Clevenger, B. Arcot, D. A. Smith, and J. M. E. Harper, "Role of stress relief in the hexagonal-close-packed to face-centered-cubic phase transformation in cobalt thin films," J. Vac. Sci. Technol., A **11**, 1435–1440 (1993).

[25] B. Zutter, M. Mecklenburg, H. L. Chan, and B. C. Regan, "Correlation of joule heating and electromigration-induced mass transport within nanoscale Co interconnects by *in situ* STEM," Microsc. Microanal. **26**, 152–154 (2020).

[26] G. J. Van Gurp, "Electromigration in cobalt films," Thin Solid Films **38**, 295–311 (1976).